THE JOURNAL OF PHYSICAL CHEMISTRY B

Article

Cite This: J. Phys. Chem. B 2019, 123, 10709−10717

pubs.acs.org/JPCB

Coaction of Electrostatic and Hydrophobic Interactions: Dynamic Constraints on Disordered TrkA Juxtamembrane Domain

Zichen Wang,[†,⊥] Huaxun Fan,[‡] Xiao Hu,[§] John Khamo,[‡] Jiajie Diao,[*,§] Kai Zhang,[*,‡,∥,#] and Taras V. Pogorelov[*,†,∥,⊥,#]

[†]Department of Chemistry, [‡]Department of Biochemistry, [∥]Center for Biophysics and Quantitative Biology, [⊥]National Center for Supercomputing Applications, and [#]Beckman Institute for Advanced Science and Technology, University of Illinois at Urbana−Champaign, Urbana, Illinois 61801, United States

[§]Department of Cancer Biology, University of Cincinnati College of Medicine, Cincinnati, Ohio 45267, United States

Supporting Information

ABSTRACT: In the receptor tyrosine kinase family, conformational change induced by ligand binding is transmitted across the membrane via a single transmembrane helix and a flexible juxtamembrane domain (JMD). Membrane dynamics makes it challenging to study the structural mechanism of receptor activation experimentally. In this study, we employ all-atom molecular dynamics with highly mobile membrane mimetic (HMMM) to capture the native conformation of the JMD in tropomyosin receptor kinase A (TrkA). We find that phosphatidylinositol 4,5-bisphosphate (PIP_2) lipids engage in stable binding with multiple basic residues. Anionic lipids can compete with salt bridges within the peptide and alter TrkA-JMD conformation. We discover three-residue insertion into the membrane and are able to either enhance or reduce the level of insertion through computationally-designed point mutations. The vesicle-binding experiment supports computational results and indicates that hydrophobic insertion is comparable to electrostatic binding for membrane anchoring. Biochemical assays on cell lines with mutated TrkA show that enhanced TrkA-JMD insertion promotes receptor degradation but does not affect the short-term signaling capacity. Our joint work points to a scenario where lipid headgroups and tails interact with basic and hydrophobic residues on disordered domain, respectively, to restrain flexibility and potentially modulate protein function.

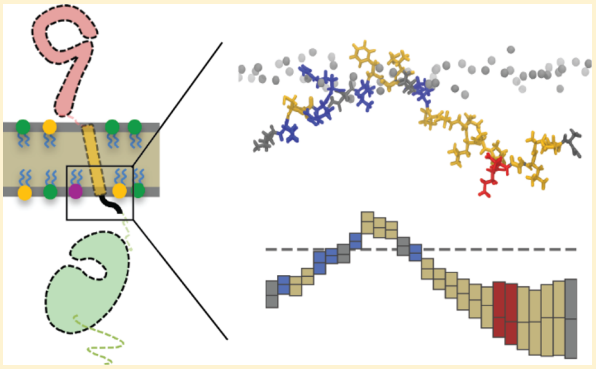

INTRODUCTION

Effective transmembrane signaling is vital to cellular decision-making. The family of receptor tyrosine kinase (RTK) contains 58 membrane proteins that dimerize upon ligand binding, induce autophosphorylation in the intracellular kinase domain, and activate downstream cascades that affect cell proliferation and function. RTK can be structurally divided into the extracellular kinase ligand-binding ectodomain, single-pass transmembrane domain (TMD), short intracellular juxtamembrane domain (JMD), and intracellular kinase domain (Figure 1a).[1] RTKs have adopted a complex regulatory role in signaling cascades[1] and are subject to transactivation by other receptors, for example, G-protein coupled receptors.[2]

Experimental studies have assigned unique functions to the JMD,[3,4] which can form secondary structures or be disordered. In particular, the JMD of the epidermal growth factor receptor (EGFR) can form a membrane-anchored helix or be part of a free antiparallel helix dimer to favor the inactive or active state, respectively.[5,6] In the fibroblast growth factor receptor 3 (FGFR3), a disordered JMD is released from being embedded in the membrane upon rotation of TMD by activating mutations.[7] JMD in some RTKs can also stabilize the unliganded dimer[8] or serve as the docking site for other cellular proteins.[9]

Common in these studies is the interplay between the JMD and the intracellular membrane. An extensive computational study[10] of all RTK JMDs reveals that the conserved positively charged JMD N-terminus actively interacts with anionic lipids such as phosphatidylinositol 4,5-bisphosphate (PIP_2). The JMDs can sequester PIP_2, effectively modifying the local membrane environment.[11−13] Moreover, PIP_2−JMD interaction has been shown to modulate receptor activity of EGFR.[14]

Tropomyosin receptor kinase A (TrkA) is well-studied for its role in neuronal differentiation and synaptic plasticity,[15] but little structural information is known regarding the activation mechanism. Deletion of a conserved Lys-Phe-Gly patch in TrkA-JMD impacts signaling activity and receptor turnover, hinting at the significance of this flexible region.[16]

Mechanistically, upon ligand binding, a conformational change is propagated from the ectodomain to TMD, which

Received: October 3, 2019
Revised: November 14, 2019
Published: November 21, 2019

DOI: 10.1021/acs.jpcb.9b09352
J. Phys. Chem. B 2019, 123, 10709−10717

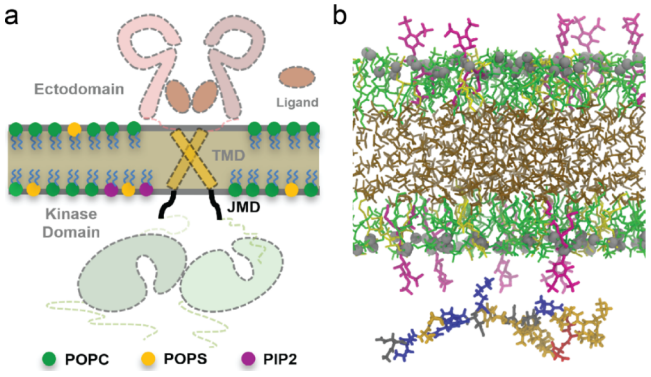

Figure 1. Overview of the system. (a) Schematic drawing of RTK dimers upon ligand binding. Domains not modeled are grayed out. (b) Snapshot of the modeled system: lipids and peptide are color-coded by type; the HMMM solvent DCLE is in brown.

by employing JMD as a flexible fulcrum, reorients the kinase domain for autophosphorylation. It is still largely unknown how this short, intrinsically disordered JMD region transduces structural change in a controlled manner. Here, we study the native conformation and membrane−protein interaction of TrkA-JMD using all-atom molecular dynamics (MD) with the highly mobile membrane-mimetic model (HMMM)[17−19] and matching experiments. TMD and kinase domain are truncated at this stage to reduce drag and improve sampling, as well as to avoid additional variables. The characterization of isolated JMD will be the first step toward a mechanistic understanding of the conformational coupling between TMD rotation and kinase activation in TrkA.

METHODS

MD Simulation. *Structure Preparation.* The wild-type sequence of human-TrkA was obtained from the UniProt Knowledgebase.[20] The JMD sequence consists of 26 amino acids, residues 440−465, in the C-terminus of the TrkA-TMD. The coordinate files for the wild type and three mutants were assembled using Avogadro software[21] solvated in VMD, and equilibrated with 5-ns stimulation (Table 1).

Table 1. TrkA-JMD Sequences

WT	N-K-C-G-R-R-N-**K-F-G**-I-N-R-P-A-V-L-A-P-E-D-G-L-A-M-S
dKFG	N-K-C-G-R-R-N-I-N-R-P-A-V-L-A-P-E-D-G-L-A-M-S
FS	N-K-C-G-R-R-N-K-**S**-G-I-N-R-P-A-V-L-A-P-E-D-G-L-A-M-S
RW	N-K-C-G-R-R-N-K-F-G-I-N-**W**-P-A-V-L-A-P-E-D-G-L-A-M-S

System Assembly. Complete peptide−membrane systems were generated using webserver CHARMM-GUI.[22] Charge-neutral ACE and CT2 terminus patches were applied to the peptide. The equilibrated peptide was placed parallel and 20 Å away from the membrane (Figure 1b). The membrane was built with the HMMM membrane builder.[23] The HMMM shortens the full-length lipid tails and fills the membrane core with an organic solvent which raises lipid lateral diffusion by ten-fold, allowing enhanced conformation sampling. The lipid area scaling factor is set at 1.1, and the terminal acyl carbon number at 6. Phosphatidylcholine (PC), phosphatidylserine (PS), and PIP_2 are incorporated. Three membrane compositions were designed to explore the roles of different lipids, while mimicking the mammalian membrane.[24,25] Numbers of PC/PS/PIP_2 per leaflet were 59:0:0 for PC membrane, 40:20:0 for PC/PS membrane, and 41:12:6 for PC/PS/PIP_2 membrane. Membrane x-/y-dimensions of the systems were maintained at 65 Å × 65 Å and z-dimension at 120 Å. Extended z-dimension shields charges from the other periodic membrane leaflet. Neutralizing potassium or chloride ions were added (three chloride ions for PC, 37 potassium ions for PC/PS, and 69 potassium ions for PC/PS/PIP_2). Each replicate has approximately 45 000 atoms. For statistics, 5 replicates were made for each lipid composition and JMD peptide variant (WT, dKFG, FS, RW), totaling 60 replicates (Table S2). Each replicate was individually generated from CHARMM-GUI with randomization in initial configuration of lipids for better sampling.

Simulation Run. All simulations were performed using software NAMD2.[26] Lipids, ions, and peptides were modeled with the CHARMM36m force field refined for disordered proteins,[27] water molecules with the TIP3P model,[28] and DCLE molecules with CGenFF.[29] A restraint of 1 kcal mol^{-1} $Å^{-2}$ perpendicular to the membrane plane was applied to the carboxyl carbon atoms of each lipid tail to avoid short-tail HMMM lipids partitioning into the solution. The restraint allowed for ±3.5 Å vertical motion along the z-direction. The lateral motions of lipids were free of restraints. Short-range electrostatics and van der Waals interactions were set with a cutoff of 12 Å with switching at 10 Å. Long-range electrostatics was modeled by the particle mesh Ewald method with 1 Å grid spacing.[30,31] The SETTLE algorithm was used to restrain the hydrogen-atom bond length.[32] The NPT ensemble was chosen. The temperature was controlled at 303 K, and the pressure was controlled at 1 atm by Langevin dynamics.[33] The integration step was set at 2 fs. All equilibration before the production followed the six cycles suggested by CHARMM-GUI where force constants were gradually reduced. Each replicate was simulated for 200 ns, reaching a total of 12 μs modeling time.

Convergence Test. To validate the use of HMMM, we converted one randomly chosen WT replicate from each membrane composition to the full-tail membrane system (lipid tail types are 16:0/18:1Δ^9) and simulated for 100 ns. The insertion distance, an informative metric (see Results and Discussion), for three reporter residues that are located on regions of the peptide with distinct insertion profiles, was plotted for the combined trajectory (Figure 2). The partitioning of peptide is largely consistent between HMMM and full-tail membrane. For additional control, the same three replicates with the HMMM membrane were extended to 300 ns (Figure S1). Z-positions of the reporter residues in the extended simulations fluctuate around the same mean as in the initial 200 ns simulations, suggesting the systems were equilibrated. Root-mean-square fluctuation (RMSF) of all residues at sliding time windows confirmed that after 50 ns, relatively low RMSFs of ∼3 Å were sustained for membrane-contacting residues (Figure S2). All analyses in the Results and Discussion were performed in the 100−200 ns interval.

Trajectory Analysis. All trajectories were visually inspected in VMD.[34] Analyses were written using MDAnalysis.[35] Details can be found in the Supporting Information.

Peptide-Vesicle Binding Experiment. *Vesicle Synthesis.* Vesicles with different compositions were synthesized according to established protocols.[36] Glass vials and glass syringes were washed three times with Milli-Q water, ethanol (100%, Fisher Scientific, USA), and chloroform (Fisher Scientific, USA) before use. Lipids (Avanti Polar Lipids, Inc, USA) were

DOI: 10.1021/acs.jpcb.9b09352
J. Phys. Chem. B 2019, 123, 10709−10717

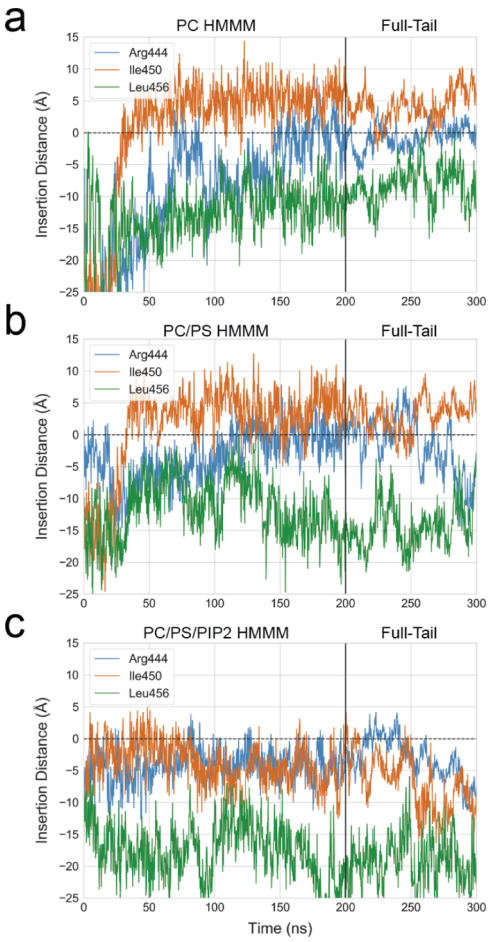

Figure 2. Comparison between the WT residue partitioning in HMMM and full-tail membrane for (a) PC, (b) PC/PS, and (c) PC/PS/PIP_2 membrane. Arg444, Ile450, and Leu456 are chosen for their distinct insertion profiles, as characterized in the Results and Discussion. The insertion distance is calculated as the z-axis difference between the whole residue center of mass and the average position of glycerol phosphorus atoms (horizontal dashed line). The positive value corresponds to membrane insertion.

added into the cleaned glass vial by the glass syringe and dried under vacuum overnight. The glass vial was wrapped with aluminum foil with a small hole on the top. Upon drying, the formed film on the glass vial was dissolved with 200 μL of 50 mM tris buffered saline (pH 8.0). The synthesized vesicle was diluted to designated concentrations and sonicated by an ultrasonic liquid processor (Misonix, USA) for 2 min (amplitude: 10%, process time: 2 s, and quiet time: 4 s) (Table 2).

Slide Preparation. The quartz slides (with drilled holes, 1 in. × 3 in., 1 mm thick, Finkenbeiner Inc, USA) and the cover slides (24 mm × 40 mm, Corning, USA) were coated with biotin-polyethylene glycol (biotin-PEG) and PEG in order to eliminate nonspecific binding of vesicles, as well as to generate biotin-NeutrAvidin bridges on the surface. The biotin-PEG and PEG were covalently immobilized onto the slide surface, according to the established protocol.[37] Briefly, the slides were thoroughly cleaned with household detergent, Milli-Q water, acetone (Fisher Scientific, USA), 1 M potassium hydroxide (Fisher Scientific, USA), and methanol (99.8%, Fisher Scientific, USA) for 1 h each. Each quartz slide was burnt with a propane torch, incubated in methanol containing with 1% (v/v) 3-aminopropyltriethoxysilane (Sigma, USA) and 5% (v/v) acetone, and coated with m-PEG-SVA and biotin-PEG-SVA (Laysan Bio Inc, USA). The flow chamber was assembled from the biotin-PEG-coated quartz slide and a cover slide using double-sided tape and epoxy glue.

Table 2. Vesicle Compositions

	DOPC (mol %)	DOPS (mol %)	PIP_2 (mol %)	biotin-PE (mol %)
vesicle 1	99.8	0	0	0.2
vesicle 2	64.8	35	0	0.2
vesicle 3	94.8	0	5	0.2

Sample Immobilization. Fifty microliter (50 μL) of 0.1 mg/mL NeutrAvidin (Fisher Scientific, USA) was incubated in the channels for 5 min at room temperature, followed by a thorough washing of the unbound NeutrAvidin. Fifty microliter (50 μL) vesicles were incubated in the channel for 40 min at room temperature, and unbound vesicles were washed out with 200 μL T50 buffer. Fifty microliter (50 μL) of Cy3 labeled RW, FS, or WT peptides (78.0, 90.0 and 75.3%, Genscript, China) were injected into separated channels, incubated for 15 min at room temperature, and then unbound peptides were washed out with 200 μL T50 buffer. Before imaging, 50 μL of oxygen scavenger solution [0.1 mg/mL glucose oxidase (Sigma, USA), 0.02 mg/mL catalase (Sigma, USA) and 0.8% (w/w) dextrose (Sigma, USA), and 3 mM 6-hydroxy-2,5,7,8-tetramethyl-chroman-2-carboxylic acid (Trolox, Sigma, USA)] were injected into each channel to eliminate single-molecule blinking.

Single-Molecule Imaging. The binding events between the vesicles and the peptides were recorded with total internal reflection fluorescence microscopy. DiD-labeled vesicles were excited at 633 nm, and the Cy3-labeled peptides were excited at 532 nm. Twenty frames of image stack were acquired with 200 ms exposure time. Real-time image analysis was done using the custom software obtained from Dr. Taekjip Ha's group at Johns Hopkins University.

Immunoblot Experiment. *Cell Culture and Transfection.* SH-SY5Y cells were cultured in Dulbecco's modified Eagle's medium (DMEM)/F12K 50/50 supplemented with 10% fetal bovine serum (FBS) and 1× penicillin−streptomycin solution (complete medium) in 35 mm tissue culture dishes were maintained in a standard humidified incubator at 37 °C with 5% CO_2. For Western blots, 600 ng of DNA was combined with 1.8 μL TurboFect in 60 μL of serum-free DMEM/F12K 50/50. The transfection mixtures were incubated at room temperature for 20 min prior to adding to cells cultured in 35 mm dishes with 2 mL complete medium. The transfection medium was replaced with 2 mL complete medium after 3 h of transfection to recover cells overnight. As for HEK293T cells, the medium for culture was DMEM supplemented with 10% FBS and 1× penicillin−streptomycin solution (complete medium), and transfection mixtures were made with serum-free DMEM.

Western Blot. SH-SY5Y cells were washed once with 1 mL cold DPBS and changed to 1 mL serum-free DMEM/F12K 50/50 medium with 1× penicillin−streptomycin solution to minimize the base-level ERK activation induced by serum. After starvation for 5 h, 20 μg cycloheximide was added directly to the medium and incubated for 1 h before NGF stimulation (1000 ng/mL final concentration). Cells were then lysed with 100 μL cold lysis buffer (RIPA + protease/

DOI: 10.1021/acs.jpcb.9b09352
J. Phys. Chem. B 2019, 123, 10709−10717

phosphatase cocktail) at 0, 10, 90, and 180 min. Lysates were centrifuged at 17 000 RCF for 10 min at 4 °C, and the suspension was collected. Purified lysates were normalized using the Bradford reagent (Thermo Fisher Scientific #23238). Equal amount of samples was mixed with LDS buffer and loaded onto 10 or 12% polyacrylamide gels. Sodium dodecyl sulfate-polyacrylamide gel electrophoresis was performed at room temperature with a cold water bath. Samples were transferred to poly(vinylidene difluoride) membranes at 30 V overnight or 80 V for 90 min at 4 °C. Membranes were blocked in 5% BSA/TBST for 1 h at room temperature and probed with the primary and secondary antibodies, according to manufacturer protocol. Membranes were incubated with the ECL substrate and imaged using a Bio-Rad ChemiDoc XRS chemiluminescence detector (BioRad). As for HEK293T cells, serum-free DMEM with 1× penicillin−streptomycin solution was used for starvation, and all the rest procedure was the same.

Quantification of Protein Level. The band intensity was analyzed by ImageJ. The level of HA-TrkA and pERK was normalized with the intensity of GAPDH in each lane. Student t-test was done using GraphPad Prism.

RESULTS AND DISCUSSION

Hydrophobic Interactions. To probe the conformations of TrkA-JMD bound to different membranes, we calculated the distances between the membrane closer to the peptide and the center of mass of each residue (Figure 3—PC/PS; Figures S3 and S4—PC, PC/PS/PIP_2). The membrane position is determined by the average *z*-position of lipid glycerol phosphorus atoms. Basic residues (blue) in the N-terminus (left in Figure 3a) predominantly interact with lipid head groups, as evidenced by their partitioning just below the glycerol phosphorus atoms. However, in all three membrane types, residues Phe448, Gly449, and Ile450 are partitioned beyond the head-water interfacial region and caged by the edge of hydrocarbon tails. This behavior is defined as membrane insertion in further discussion. Residues C-terminal (right in Figure 3a) to Arg452 barely interact with the membrane and are suspended in water. The broad interquartile range for residues on the C-terminus indicates high flexibility caused by the truncation of the kinase domain as well as the inability to insert. The insertion distance plot can be visualized as the ensemble-average conformation relative to the membrane, which resembles the actual structure (Figure 3b) and offers information on the degree of fluctuation.

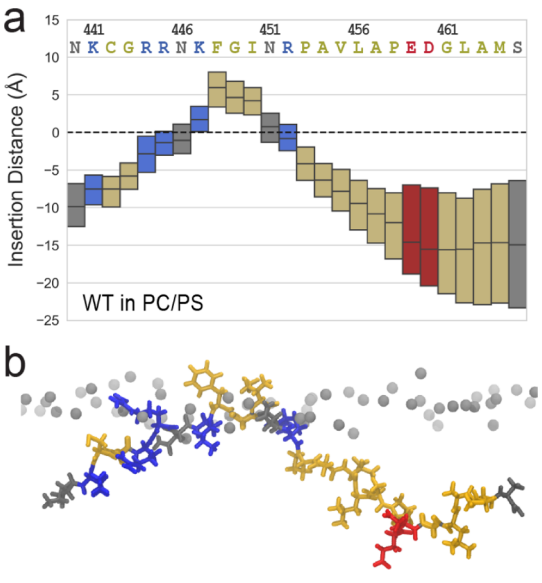

Figure 3. TrkA-JMD insertion into the membrane. (a) Insertion distance is calculated as the *z*-axis difference between the whole residue center of mass and the average position of glycerol phosphorus atoms (horizontal dashed line) in the PC/PS membrane. Data points collected from the last 50 ns are presented as box plot, and three quartiles are shown. Boxes and the sequence are color-coded by the residue type: yellow—hydrophobic, gray—polar, blue—basic, and red—acidic. (b) A snapshot of peptide insertion: the membrane core is on the top; phosphorus atoms are gray spheres.

To investigate the significance of hydrophobic insertion and charge interaction, we designed three JMD mutations. First, Lys447, Phe448, and Gly449 were deleted (dKFG), as in previous studies in mammalian cell culture.[16] Second, Phe448 was mutated to Ser448 (FS) to remove the favorable aromatic ring insertion. Third, Arg452 was substituted with Trp452 (RW) to replace charge interactions with hydrophobic interactions. The mutant systems were simulated with the same protocols as the WT. In dKFG and FS, the removal of membrane-associative residues Lys447 and Phe448 or the introduction of polar residue Ser448 eliminates insertion and leaves electrostatic anchoring alone. In RW, the loss of basic Arg452 is compensated by the introduced Trp452 insertion (Figure 4). As a result, in addition to F-G-I insertions, residues 452−456 are partially embedded within the membrane. RW mutation also induces more fluctuation than the native sequence. Similar binding patterns were observed for other membrane compositions (Figures S3 and S4), and convergence was mostly achieved as different replicates yield similar boxplots (Figure S5).

To validate the computational findings, we used a single-molecule peptide-liposome binding assay to evaluate the binding affinity between DiD-labeled, composition-controlled lipids, and Cy3-labeled JMD peptides (Figure 4b). Full-coverage vesicles were prepared to eliminate nonspecific interactions between peptides and the PEG-coated surface (Figure S8). The peptide-vesicle binding affinity was directly proportional to the number of Cy3 fluorescent spots in a field of view. Enhanced peptide binding was seen in PC/PS and PC/PIP_2 vesicles with 1 μg/mL of peptide. The number of detected spots increases from FS to WT to RW (Figure 4c), suggesting that the partition susceptibility of JMD binding to anionic membrane ranks as FS < WT < RW. This result agrees with the insertions predicted by MD simulations. From the count differences between vesicles, we concluded that long-range electrostatics promotes peptide binding. However, once the binding is achieved, the extent of hydrophobic insertion significantly affects the strength of binding. The PC-only membrane is likely too neutral for peptide to attach in the experiment (Figure S9), while the separation is small enough to allow peptide binding to the PC membrane in the simulation.

TrkA-JMD conformation is distinct from experimentally[3] and computationally[6] characterized EGFR-JMD conformations: EGFR-JMD forms a short but structured 9-residue helix from Leu679 to Glu687 that can be membrane-embedded, while the corresponding Ile450 to Pro458 residues in TrkA-JMD are disordered and suspended in water. The disordered structure is also supported by secondary structure prediction webservers.[38,39] In the N-terminus, in addition to the strong

DOI: 10.1021/acs.jpcb.9b09352
J. Phys. Chem. B 2019, 123, 10709−10717

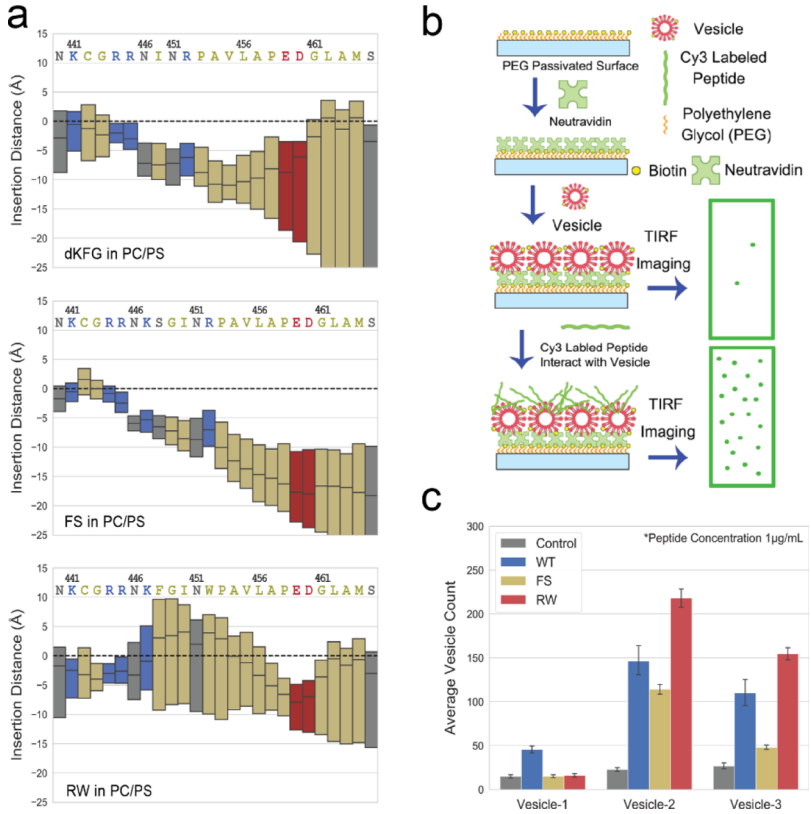

Figure 4. Role of mutations in TrkA-JMD binding. (a) Insertion distance for dKFG, FS, and RW mutants in the PC/PS membrane. (b) Illustration of the surface functionalization and single-molecule imaging of specific bound peptide on vesicles immobilized on the channel surface. (c) Fluorophore counts of Cy3-labeled peptides bound with different vesicles at peptide concentration equal to 1 μg/mL. Vesicle compositions: vesicle-1 100% DOPC, vesicle-2 65% DOPC and 35% DOPS, vesicle-3 95% DOPC, and 5% PIP_2. Error bars denote 95% confidence interval.

electrostatic binding because of the conserved presence of basic residue, TrkA-JMD possesses stable hydrophobic insertion unseen in EGFR-JMD. Even though HMMM is different from the full-tail membrane, free energy changes of side-chains membrane insertion agree well among the two models.[40] Interestingly, the experimental Wimley–White hydrophobicity scale[41] gives similar predictions on the insertion profiles characterized by MD-HMMM simulations. The Wimley–White scale provides the free energy change of partitioning a whole residue into the PC membrane using pentapeptide AcWL-X-LL, describing the tendency of X for membrane insertion. To avoid confusion, it is worth noting that basic residue association with the anionic membrane is a different scenario and not expected to follow the positive free energies given by the scale.

To list the relevant residues, Phe and Trp have negative free energies of −1.13 and −1.85 kcal/mol, respectively. Ser, Pro, Ala, and Val have positive free energies of 0.13, 0.45, 0.17, and 0.07 kcal/mol, respectively, because of the unfavorable contribution from the polar peptide bond. These free energy values are consistent with the following computational results: (1) in WT, Phe448 engages in stable insertion, yet residues after Arg452 do not; (2) FS mutation completely removes insertion; (3) RW mutation is highly favorable and compensate for the loss of basic–lipid interaction and even promotes insertion of additional residues. Though the Wimley–White scale is obtained for the PC-only membrane, our simulations indicate similar patterns of insertion in anionic membranes. Altogether, in addition to previously characterized electrostatic binding between JMD and anionic membranes,[7,10−13] our results suggest that hydrophobic insertions also contribute to the membrane anchoring and stabilization of N-terminal TrkA-JMD.

Electrostatic Interactions. To explore protein–lipid interaction as is evident from the membrane partitioning of N-terminus, contacts between lipid-charged moieties and residues 440–452 were mapped. The mean contact number measures the average number of contacting lipids at a given frame. The mean contact number for the WT confirms that most contacts were formed with the basic residues (Figure 5a, see Figure S6 for mutants). Considering the amounts of lipids present are nearly equal, stronger charge interaction is formed in PC/PS, PC/PS/PIP_2 membranes (on average two lipids per basic residue) than in the PC membrane (one lipid per basic residue). Mean contact duration measures the average time a lipid stays in contact with the residue side-chain before it dissociates. Mean contact duration for each type of lipid is calculated for the PC/PS/PIP_2 membrane in contact with the WT (Figure 5b, see Figure S7 for mutants). The average binding time of PIP_2 is on the order of tens of nanoseconds, in stark contrast to the short-lived contacts by PC and PS lipids.

To address the role of differently charged lipids, we analyzed contacts formed between residues on JMD. The contacts were evaluated in fraction of contact pairs, and the average occurrence of two-residue contacts divided by the number of possible pairs to be formed (Figure 5c). Particularly, contacts between any of acidic Glu459, Asp460, and any of the basic residues (vary in WT and mutants) are shown to be present in the PC-only membrane but not in the more charged membranes. Though considerable replicate-level variation

DOI: 10.1021/acs.jpcb.9b09352
J. Phys. Chem. B 2019, 123, 10709−10717

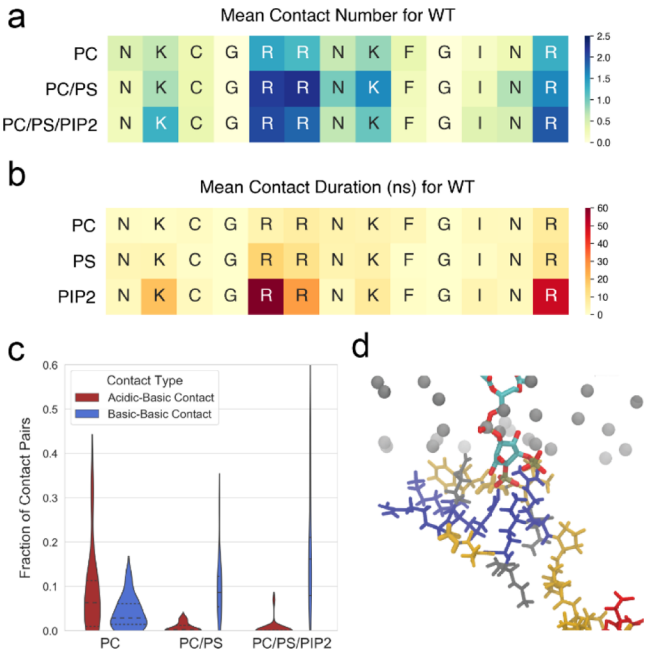

Figure 5. Molecular characterization of JMD-lipid interactions. (a) Mean contact number for three membranes and 13 residues in the N-terminus of the WT JMD. (b) Mean contact duration for three types of lipids in PC/PS/PIP_2 and 13 residues in the N-terminus of the WT JMD. (c) The fraction of contact pairs for acidic−basic and basic−basic contacts on wide-type and mutant JMD is presented as the violin plot. An average value is calculated for each replicate in wild-type and mutant systems. The width of the violin is proportional to the number of data points. Quartiles are shown as dashed lines. (d) A snapshot of PIP_2 inositol phosphates coordinating three JMD basic residues.

exists as each violin plot contains only 20 data points, contacts between basic residues are more frequent in negatively charged membranes. In some replicates, PIP_2 is capable of coordinating more than two residues (Figure 5d).

In all three lipid compositions, the JMD peptide rapidly forms an encounter complex with the membrane from the initial position 20 Å away. This membrane attachment of JMD N-terminus through long-range charge interaction is necessary for membrane insertion, as suggested by the vesicle-binding experiment. Although PS and PIP_2 lipids exhibit enhanced charge interaction (Figure 5a), PS lipids tend to form frequent yet transient contacts, while PIP_2 lipids persistently bind to basic residues (Figure 5b). With the addition of anionic lipids, fold-increase of basic−basic residue contacts in JMD is observed (Figure 5d). Combined with the contact analysis, the results point to a distinct mode of PIP_2−peptide interactions, where two phosphate groups on the inositol ring coordinate more than one basic residue for prolonged time (tens of nanoseconds).

The primary effect of membrane composition on TrkA-JMD conformation can be seen on the C-terminus where acidic residues reside. This region tends to be more flexible and distal from the membrane as the amount of anionic lipids increases (Figures 3a,b, S3, S4). One factor is the repulsion between acidic residues and enriched negative charge in the membrane. Another factor is the competition between anionic lipids and JMD acidic residues to bind basic residues. As more anionic lipids are included, acid-basic residue contacts that loop the C-terminus closer to the membrane get depleted (Figure 5d). This effect would be significant if the orientation of JMD C-terminus in turn affects the orientation of downstream kinase domain. The interplay between membrane composition and JMD orientation might potentially explain the relative conservation of acidic residues on the C-terminal patch of JMD in all RTKs.[10]

Full Receptor Function. Because TrkA-JMD is involved in NGF-mediated receptor degradation,[16] we hypothesize that mutations altering JMD-membrane interactions can affect in-cell degradation kinetics. To test this hypothesis, we transfected SH-SY5Y human neuronal cells with wild-type (WT) and mutant (FS, RW) hTrkA fused with a human influenza hemagglutinin tag (hTrkA-HA). Twenty-four hours after

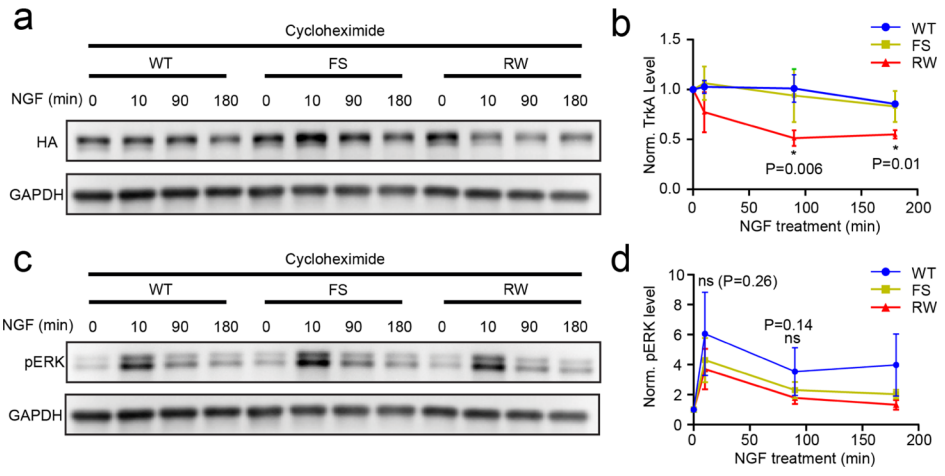

Figure 6. Quantitative determination of the degradation kinetics and signaling activity for the WT, FS, and RW HA-hTrkA mutants in SHSY5Y cells. (a) Western blot analysis of TrkA abundance probed with an anti-HA antibody. Serum-deprived cells were pretreated with cycloheximide to block new protein synthesis, followed by 100 ng/mL NGF treatment for 0, 10, 90, and 180 min. GAPDH was used as a loading control. (b) Quantification of the TrkA level normalized over the GAPDH level from three replicates. The RW mutant shows significantly faster degradation kinetics than the WT and FS mutants. (c) Western blot analysis of the NGF-mediated ERK signaling activation in SHSY5Y cells. Cells were treated the same as in (a). (d) Quantification of the pERK level normalized over the GAPDH level from three replicates. No significant difference was detected between WT and two TrkA mutants.

DOI: 10.1021/acs.jpcb.9b09352
J. Phys. Chem. B 2019, 123, 10709−10717

transfection, cells were starved in serum-free medium for 6 hours prior to treatment with the nerve growth factor (NGF). Cycloheximide was applied 1 h before NGF treatment, and Western blot analysis against HA was used to monitor the intracellular level of TrkA. The abundance of WT- and FS-hTrkA-HA decreased to approximately 80% 180 min after NGF treatment (Figure 6a, S10). The RW mutant, on the other hand, showed significantly faster degradation kinetics, as evidenced by the 50% pretreatment level as short as 90 min after NGF treatment (Figure 6b, S10). Variation of the hTrkA abundance should not arise from unequal loading because the level of the GAPDH (loading control) protein from the same blot was comparable between replicates. This result suggests that RW mutation accelerates the NGF-mediated degradation kinetics of hTrkA, given that an equal amount of WT and mutant hTrkA was transfected.

Endocytosis of TrkA that results in endosome degradation or receptor recycling is triggered by NGF-induced ubiquitination performed by multiple E3 ligases.[42−44] Lys447 is mono-ubiquitinated, and its deletion causes resistance to degradation.[16,44] Our insertion analysis shows that Lys447 is membrane inserted for half of the simulation time in the WT and RW (likely driven by Phe448) but is free in the FS. Intriguingly, our in-cell results suggest that the degradation kinetics of FS is similar to that of WT (Figure 6b), even though in the FS mutant, Lys447 is more exposed to the solvent. The finding that RW mutation promotes ubiquitination is subject to at least two explanations: (1) the insertion profile of residues downstream Lys447 affects substrate recognition of the E3 ligase, likely Cbl-b;[44] (2) because ubiquitination occurs after receptor activation, the active JMD conformation is altered by RW mutation but differs from our computational prediction of free JMD. This finding may guide future studies that probe the TrkA conformational change upon activation.

Prior studies suggest that JMDs in EGFR and FGFR3 can switch from the membrane-embedded state to the free-floating state, depending on TMD dimer tilt angles.[5−7] Inspired by these findings, we hypothesize that the mutant FS and RW will change inherent TrkA activity by reducing and enhancing JMD binding affinity to the membrane, shifting the equilibrium to favor one state. Prior experiments showed that the dKFG mutation induces more robust signaling,[16] which correlates with our hypothesis and computational observation of altered membrane insertion (Figure 4a). However, after NGF binding activates the downstream Ras/ERK (extracellular signal regulated kinase) pathway, the FS and RW mutants show similar fold increases of pERK activity as the WT (Figure 6c−d). To account for background noise from indigenous TrkA in SH-SY5Y cell-line, we repeat in HEK293T cell-line that does not express indigenous TrkA or degradation machinery. The data confirm that the difference in the signaling capacity of WT/FS/RW-TrkA cannot be resolved from noise up to 3 h (Figure S11). Although here we computationally reported the behavior of truncated TrkA-JMD, in-cell experiments suggest the role of JMD in the full receptor can be more involved and require further investigation.

CONCLUSIONS

Using all-atom MDs, we highlighted the roles of hydrophobic and electrostatic binding in peptide−membrane interactions. We recovered the strong charge-driven interactions between anionic lipids and basic residues in TrkA-JMD N-terminus, previously emphasized by coarse-grained studies. With increased concentrations of PS and PIP_2 lipids, higher lipid contact number is observed. We also found PIP_2 engages in stable binding (tens of nanoseconds) to two or more basic residues. As the PIP_2 becomes enriched in the membrane, this lipid−protein interaction diminishes salt bridges in TrkA-JMD that are responsible for placing the C-terminus adjacent to the membrane. In the full-length receptor, the C-terminus is attached to the kinase domain, and reorientation of the kinase domain activates autophosphorylation. For these facts, we proposed that anionic lipids can potentially affect signaling activity by pushing off the C-terminus and reorienting the JMD to form a larger angle with respect to the membrane plane.

In addition to electrostatic interactions, we characterized the TrkA-JMD insertion profiles, which agree with the experimental Wimley & White hydrophobicity scale. We revealed a highly stable F-G-I insertion in the JMD N-terminus. Substituting the phenylalanine with serine abolishes insertion, while replacing an arginine to tryptophan results in more insertions. Vesicle-binding experiment supported computational predictions and showed that hydrophobic insertion is comparable to electrostatic binding in membrane association. The results suggest a peptide−membrane binding strategy where long-range electrostatics brings the domain near the membrane for favorable hydrophobic patch to hook to it. Studies on EGFR and FGFR3 activation mechanism assigned different levels of JMD insertion to active/inactive states. We then hypothesized that perturbations on JMD insertion should change the inherent receptor response to the ligand. However, biochemical assays on cell lines with mutated human TrkA only showed differences in the degradation kinetics but not in the short-term signaling capacity. This evidence indicates that TrkA-JMD assumes a more convoluted role in signaling. Further studies should incorporate the effect of TMD, kinase domain, and dimerization in order to better elucidate the structural basis of receptor activation.

ASSOCIATED CONTENT

Supporting Information

The Supporting Information is available free of charge at https://pubs.acs.org/doi/10.1021/acs.jpcb.9b09352.

Supplementary tables, supplementary figures, and supplementary methods (PDF)

AUTHOR INFORMATION

Corresponding Authors

*E-mail: jiajie.diao@uc.edu (J.D.).
*E-mail: kaizkaiz@illinois.edu (K.Z.).
*E-mail: pogorelo@illinois.edu (T.V.P.).

ORCID

Zichen Wang: 0000-0003-4759-3053
Huaxun Fan: 0000-0003-3657-9758
Xiao Hu: 0000-0001-9133-3705
John Khamo: 0000-0001-7179-0589
Jiajie Diao: 0000-0003-4288-3203
Kai Zhang: 0000-0002-6687-4558
Taras V. Pogorelov: 0000-0001-5851-7721

Notes

The authors declare no competing financial interest.

DOI: 10.1021/acs.jpcb.9b09352
J. Phys. Chem. B 2019, 123, 10709−10717

■ ACKNOWLEDGMENTS

T.V.P. acknowledges support from the Department of Chemistry, the School of Chemical Sciences, and the Office of the Vice-Chancellor for Research (RSOCR Award 4703) at University of Illinois at Urbana-Champaign. T.V.P. acknowledges computational resources from the Texas Advanced Computing Center (TACC) at the University of Texas at Austin made available from the Extreme Science and Engineering Discovery Environment (XSEDE) Grant TG-MCB130112, which is supported by National Science Foundation Grant ACI-1053575. K.Z. acknowledges support from the School of Molecular and Cellular Biology at UIUC and NIH (1R01GM132438). J.D. acknowledges support from NIH (R35GM128837). Z.W. acknowledges support from Student Pushing Innovation (SPIN) Program of the National Center for Supercomputing Applications (NCSA). The authors are grateful to Dr. Yekaterina (Katka) Golubeva for assistance with the RTK schematics.

■ REFERENCES

(1) Lemmon, M. A.; Schlessinger, J. Cell Signaling by Receptor-Tyrosine Kinases. *Cell* **2010**, *141*, 1117−1134.
(2) Zhou, R.; Han, B.; Xia, C.; Zhuang, X. Membrane-Associated Periodic Skeleton Is a Signaling Platform for RTK Transactivation in Neurons. *Science* **2019**, *365*, 929−934.
(3) Jura, N.; Endres, N. F.; Engel, K.; Deindl, S.; Das, R.; Lamers, M. H.; Wemmer, D. E.; Zhang, X.; Kuriyan, J. Mechanism for Activation of the EGF Receptor Catalytic Domain by the Juxtamembrane Segment. *Cell* **2009**, *137*, 1293−1307.
(4) He, L.; Hristova, K. Consequences of Replacing EGFR Juxtamembrane Domain with an Unstructured Sequence. *Sci. Rep.* **2012**, *2*, 854.
(5) Endres, N. F.; Das, R.; Smith, A. W.; Arkhipov, A.; Kovacs, E.; Huang, Y.; Pelton, J. G.; Shan, Y.; Shaw, D. E.; Wemmer, D. E.; et al. Conformational Coupling across the Plasma Membrane in Activation of the EGF Receptor. *Cell* **2013**, *152*, 543−556.
(6) Arkhipov, A.; Shan, Y.; Das, R.; Endres, N. F.; Eastwood, M. P.; Wemmer, D. E.; Kuriyan, J.; Shaw, D. E. Architecture and Membrane Interactions of the EGF Receptor. *Cell* **2013**, *152*, 557−569.
(7) Tamagaki, H.; Furukawa, Y.; Yamaguchi, R.; Hojo, H.; Aimoto, S.; Smith, S. O.; Sato, T. Coupling of Transmembrane Helix Orientation to Membrane Release of the Juxtamembrane Region in FGFR3. *Biochemistry* **2014**, *53*, 5000−5007.
(8) Sarabipour, S.; Hristova, K. FGFR3 Unliganded Dimer Stabilization by the Juxtamembrane Domain. *J. Mol. Biol.* **2015**, *427*, 1705−1714.
(9) Sengupta, P.; Bosis, E.; Nachliel, E.; Gutman, M.; Smith, S. O.; Mihályné, G.; Zaitseva, I.; McLaughlin, S. EGFR Juxtamembrane Domain, Membranes, and Calmodulin: Kinetics of Their Interaction. *Biophys. J.* **2009**, *96*, 4887−4895.
(10) Hedger, G.; Sansom, M. S. P.; Koldsø, H. The Juxtamembrane Regions of Human Receptor Tyrosine Kinases Exhibit Conserved Interaction Sites with Anionic Lipids. *Sci. Rep.* **2015**, *5*, 9198.
(11) Halim, K. B. A.; Koldsø, H.; Sansom, M. S. P. Interactions of the EGFR Juxtamembrane Domain with PIP2-Containing Lipid Bilayers: Insights from Multiscale Molecular Dynamics Simulations. *Biochim. Biophys. Acta* **2015**, *1850*, 1017−1025.
(12) Chavent, M.; Karia, D.; Kalli, A. C.; Domański, J.; Duncan, A. L.; Hedger, G.; Stansfeld, P. J.; Seiradake, E.; Jones, E. Y.; Sansom, M. S. P. Interactions of the EphA2 Kinase Domain with PIPs in Membranes: Implications for Receptor Function. *Structure* **2018**, *26*, 1025−1034.e2.
(13) McLaughlin, S.; Smith, S. O.; Hayman, M. J.; Murray, D. An Electrostatic Engine Model for Autoinhibition and Activation of the Epidermal Growth Factor Receptor (EGFR/ErbB) Family. *J. Gen. Physiol.* **2005**, *126*, 41−53.
(14) Michailidis, I. E.; Rusinova, R.; Georgakopoulos, A.; Chen, Y.; Iyengar, R.; Robakis, N. K.; Logothetis, D. E.; Baki, L. Phosphatidylinositol-4,5-Bisphosphate Regulates Epidermal Growth Factor Receptor Activation. *Pflugers Arch. Eur. J. Physiol.* **2011**, *461*, 387−397.
(15) Huang, E. J.; Reichardt, L. F. Trk Receptors: Roles in Neuronal Signal Transduction. *Annu. Rev. Biochem.* **2003**, *72*, 609−642.
(16) Kiris, E.; Wang, T.; Yanpallewar, S.; Dorsey, S. G.; Becker, J.; Bavari, S.; Palko, M. E.; Coppola, V.; Tessarollo, L. TrkA in Vivo Function Is Negatively Regulated by Ubiquitination. *J. Neurosci.* **2014**, *34*, 4090−4098.
(17) Ohkubo, Y. Z.; Pogorelov, T. V.; Arcario, M. J.; Christensen, G. A.; Tajkhorshid, E. Accelerating Membrane Insertion of Peripheral Proteins with a Novel Membrane Mimetic Model. *Biophys. J.* **2012**, *102*, 2130−2139.
(18) Vermaas, J. V.; Baylon, J. L.; Arcario, M. J.; Muller, M. P.; Wu, Z.; Pogorelov, T. V.; Tajkhorshid, E. Efficient Exploration of Membrane-Associated Phenomena at Atomic Resolution. *J. Membr. Biol.* **2015**, *248*, 563−582.
(19) Baylon, J. L.; Vermaas, J. V.; Muller, M. P.; Arcario, M. J.; Pogorelov, T. V.; Tajkhorshid, E. Atomic-Level Description of Protein-Lipid Interactions Using an Accelerated Membrane Model. *Biochim. Biophys. Acta, Biomembr.* **2016**, *1858*, 1573−1583.
(20) The Uniprot Consortium. UniProt: A Worldwide Hub of Protein Knowledge. *Nucleic Acids Res.* **2019**, *47*, D506−D515.
(21) Hanwell, M. D.; Curtis, D. E.; Lonie, D. C.; Vandermeerschd, T.; Zurek, E.; Hutchison, G. R. Avogadro: An Advanced Semantic Chemical Editor, Visualization, and Analysis Platform. *J. Cheminf.* **2012**, *4*, 17.
(22) Jo, S.; Kim, T.; Iyer, V. G.; Im, W. CHARMM-GUI: A Web-Based Graphical User Interface for CHARMM. *J. Comput. Chem.* **2008**, *29*, 1859−1865.
(23) Qi, Y.; Cheng, X.; Lee, J.; Vermaas, J. V.; Pogorelov, T. V.; Tajkhorshid, E.; Park, S.; Klauda, J. B.; Im, W. CHARMM-GUI HMMM Builder for Membrane Simulations with the Highly Mobile Membrane-Mimetic Model. *Biophys. J.* **2015**, *109*, 2012−2022.
(24) van Meer, G.; Voelker, D. R.; Feigenson, G. W. Membrane Lipids: Where They Are and How They Behave. *Nat. Rev. Mol. Cell Biol.* **2008**, *9*, 112−124.
(25) Zachowski, A. Phospholipids in Animal Eukaryotic Membranes: Transverse Asymmetry and Movement. *Biochem. J.* **1993**, *294*, 1−14.
(26) Phillips, J. C.; Braun, R.; Wang, W.; Gumbart, J.; Tajkhorshid, E.; Villa, E.; Chipot, C.; Skeel, R. D.; Kalé, L.; Schulten, K. Scalable Molecular Dynamics with NAMD. *J. Comput. Chem.* **2005**, *26*, 1781−1802.
(27) Huang, J.; Rauscher, S.; Nawrocki, G.; Ran, T.; Feig, M.; De Groot, B. L.; Grubmüller, H.; MacKerell, A. D. CHARMM36m: An Improved Force Field for Folded and Intrinsically Disordered Proteins. *Nat. Methods* **2016**, *14*, 71−73.
(28) Jorgensen, W. L.; Chandrasekhar, J.; Madura, J. D.; Impey, R. W.; Klein, M. L. Comparison of Simple Potential Functions for Simulating Liquid Water. *J. Chem. Phys.* **1983**, *79*, 926.
(29) Vanommeslaeghe, K.; Hatcher, E.; Acharya, C.; Kundu, S.; Zhong, S.; Shim, J.; Darian, E.; Guvench, O.; Lopes, P.; Vorobyov, I.; Mackerell, A. D., Jr. CHARMM General Force Field: A Force Field for Drug-Like Molecules Compatible with the CHARMM All-Atom Additive Biological Force Fields. *J. Comput. Chem.* **2010**, *31*, 671−690.
(30) Darden, T.; York, D.; Pedersen, L. Particle Mesh Ewald: An N·log(N) Method for Ewald Sums in Large Systems. *J. Chem. Phys.* **1993**, *98*, 10089.
(31) Essmann, U.; Perera, L.; Berkowitz, M. L.; Darden, T.; Lee, H.; Pedersen, L. G. A Smooth Particle Mesh Ewald Method. *J. Chem. Phys.* **1995**, *103*, 8577.
(32) Miyamoto, S.; Kollman, P. A. Settle: An Analytical Version of the SHAKE and RATTLE Algorithm for Rigid Water Models. *J. Comput. Chem.* **1992**, *13*, 952−962.

DOI: 10.1021/acs.jpcb.9b09352
J. Phys. Chem. B 2019, 123, 10709−10717

(33) Martyna, G. J.; Tobias, D. J.; Klein, M. L. Constant Pressure Molecular Dynamics Algorithms. *J. Chem. Phys.* **1994**, *101*, 4177−4189.
(34) Humphrey, W.; Dalke, A.; Schulten, K. VMD: Visual Molecular Dynamics. *J. Mol. Graph.* **1996**, *14*, 33−38.
(35) Michaud-Agrawal, N.; Denning, E. J.; Woolf, T. B.; Beckstein, O. MDAnalysis: A Toolkit for the Analysis of Molecular Dynamics Simulations. *J. Comput. Chem.* **2011**, *32*, 2319−2327.
(36) Cai, B.; Yu, L.; Sharum, S. R.; Zhang, K.; Diao, J. Single-Vesicle Measurement of Protein-Induced Membrane Tethering. *Colloids Surf., B* **2019**, *177*, 267−273.
(37) Diao, J.; Ishitsuka, Y.; Lee, H.; Joo, C.; Su, Z.; Syed, S.; Shin, Y.-K.; Yoon, T.-Y.; Ha, T. A Single Vesicle-Vesicle Fusion Assay for in Vitro Studies of Snares and Accessory Proteins. *Nat. Protoc.* **2012**, *7*, 921−934.
(38) Drozdetskiy, A.; Cole, C.; Procter, J.; Barton, G. J. JPred4: A Protein Secondary Structure Prediction Server. *Nucleic Acids Res.* **2015**, *43*, W389.
(39) Lin, K.; Simossis, V. A.; Taylor, W. R.; Heringa, J. A Simple and Fast Secondary Structure Prediction Method Using Hidden Neural Networks. *Bioinformatics* **2005**, *21*, 152−159.
(40) Pogorelov, T. V.; Vermaas, J. V.; Arcario, M. J.; Tajkhorshid, E. Partitioning of Amino Acids into a Model Membrane: Capturing the Interface. *J. Phys. Chem. B* **2014**, *118*, 1481−1492.
(41) Wimley, W. C.; White, S. H. Experimentally Determined Hydrophobicity Scale for Proteins at Membrane Interfaces. *Nat. Struct. Biol.* **1996**, *3*, 842−848.
(42) Arévalo, J. C.; Waite, J.; Rajagopal, R.; Beyna, M.; Chen, Z.-Y.; Lee, F. S.; Chao, M. V. Cell Survival through Trk Neurotrophin Receptors Is Differentially Regulated by Ubiquitination. *Neuron* **2006**, *50*, 549−559.
(43) Takahashi, Y.; Shimokawa, N.; Esmaeili-Mahani, S.; Morita, A.; Masuda, H.; Iwasaki, T.; Tamura, J. i.; Haglund, K.; Koibuchi, N. Ligand-Induced Downregulation of TrkA Is Partly Regulated through Ubiquitination by Cbl. *FEBS Lett.* **2011**, *585*, 1741−1747.
(44) Emdal, K. B.; Pedersen, A.-K.; Bekker-Jensen, D. B.; Tsafou, K. P.; Horn, H.; Lindner, S.; Schulte, J. H.; Eggert, A.; Jensen, L. J.; Francavilla, C.; et al. Temporal Proteomics of NGF-TrkA Signaling Identifies an Inhibitory Role for the E3 Ligase Cbl-b in Neuroblastoma Cell Differentiation. *Sci. Signal.* **2015**, *8*, ra40.

DOI: 10.1021/acs.jpcb.9b09352
J. Phys. Chem. B 2019, 123, 10709−10717